# Organic Nanoflowers from a Wide Variety of Molecules Templated by a Hierarchical Supramolecular Scaffold

Luis M. Negrón, Tanya L. Díaz, Edwin O. Ortiz-Quiles, Diómedes Dieppa-Matos, Bismark Madera-Soto, and José M. Rivera*

Department of Chemistry and the Molecular Sciences Research Center, University of Puerto Rico at Río Piedras, San Juan, 00926, Puerto Rico

S *Supporting Information*
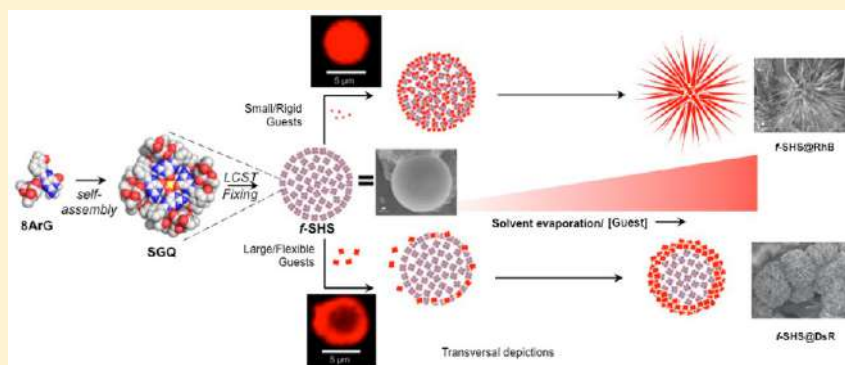
ABSTRACT: Nanoflowers (NFs) are flowered-shaped particles with overall sizes or features in the nanoscale. Beyond their pleasing aesthetics, NFs have found a number of applications ranging from catalysis, to sensing, to drug delivery. Compared to inorganic based NFs, their organic and hybrid counterparts are relatively underdeveloped mostly because of the lack of a reliable and versatile method for their construction. We report here a method for constructing NFs from a wide variety of biologically relevant molecules (guests), ranging from small molecules, like doxorubicin, to biomacromolecules, like various proteins and plasmid DNA. The method relies on the encapsulation of the guests within a hierarchically structured particle made from supramolecular G-quadruplexes. The size and overall flexibility of the guests dictate the broad morphological features of the resulting NFs, specifically, small and rigid guests favor the formation of NFs with spiky petals, while large and/or flexible guests promote NFs with wide petals. The results from experiments using confocal fluorescence microscopy, and scanning electron microscopy provides the basis for the proposed mechanism for the NF formation.

INTRODUCTION

Nanoflowers (NFs) are flower-like nano/microparticles with nanoscale features (e.g., petals) that enable applications such as catalysis,[1] sensing and drug delivery.[2−4] Relative to inorganic-based NFs, their organic and hybrid counterparts are relatively underdeveloped.[5] The lack of a general method for the preparation of NFs hinders their technological applications, since currently their preparation relies mostly on serendipity, followed by the concurrent optimization of multiple parameters like solvent, concentration, and temperature. The methodology presented here provides an alternative to fill this gap, and it illustrates the importance of using a supramolecular scaffold to seed the growth of complex flower-like structures from a wide variety of biomolecules.

The parallels between nanoflowers and their macroscopic biological/natural counterparts go beyond simple morphological characteristics. Although the basic building blocks are notably different (i.e., cells vs molecules), their ultimate morphological features depend on parameters such as the growth, anisotropy, direction, and rotation of such building blocks.[6] NFs can be classified by their size (nano/micro), and/or their morphology: rose-like, carnation-like, and dandelion-like. Alternatively, they could be classified more generally by two broad categories based on the shapes of their petals: spiky petalled or wide petalled. A common classification scheme for NFs rely on their composition, as inorganic, hybrid, and organic. Inorganic NFs are most commonly made from a wide variety of metals and other inorganic salts,[5] and the overwhelming majority of examples described in the literature are of this type. Hybrid NFs are those that contain significant proportions of both organic and inorganic components, or more commonly, those in which the main component is organic, but coordination bonds are one of the main driving forces in their formation.[1,7−10] Organic NFs are those composed exclusively of organic molecules, or those in which organic molecules are the main component and inorganic elements (e.g., salts) are present as part of the medium from which the NFs are made, but their coordination is not the main

driving force to form the resulting NFs.[3,4,11−13] Hybrid and organic NFs could be further classified by the nature of the organic component. Specifically, those made from small molecules[11−15] and those made from macromolecules.[1,4,9,10]

While the formation of macrogels by guanosine and related compounds has been recognized for over a century,[16] the corresponding colloidal micro- or nanogel versions have not been described until recently. A few years ago we discovered that the thermally triggered assembly (i.e., lower critical solution temperature, a.k.a., LCST) of supramolecular G-quadruplexes (SGQs) made from 8-aryl-2′-deoxyguanosine (8ArG) derivatives (Figure 1)[17] led to the formation of hierarchically organized colloidal particles with a gel-like interior we termed supramolecular hacky sacks (SHS). Furthermore, we demonstrated that the SHS particles are suitable for the encapsulation of guest molecules like the fluorescent anticancer drug doxorubicin (Dox).[17b] Recently, while characterizing this and other encapsulation complexes in the solid state we discovered that the SHS served as a versatile template for the formation of organic NFs. While this initial discovery was serendipitous like that of most reported NFs, the subsequent studies described in this article demonstrate that the resulting methodology (Figure 1) provides a viable alternative to prepare NFs containing a wide variety of molecules of biological importance.

■ EXPERIMENTAL SECTION

Scanning Electron Microscopy (SEM). These experiments were performed in a high-resolution field emission JEOL JSM-7500F SEM. The instrument probe was used in low current (LC) mode 10, acceleration (Accel) voltage of 2.00 kV, and emission current of 10.0 μA. The walking distance (WD) was 8.8 ± 0.1 mm at 9.5×10^{-5} Pa of vacuum with column mode used in gentle beam low (GB-L) and low magnification (LM) modes. The software used to obtain the SEM images was JEOL Serving Advanced Technology, PC-SEM Ver2, 1, 0, 3 (2006−2010).

Confocal Laser Scanning Microscopy (CLSM). These images were obtained in a Confocal Zeiss LSM 510 META on an Axiovision Z1 microscope with an excitation range of (405 nm, 458 nm, 477 nm, 488 nm, 514 nm, 561 nm, 633 nm) and emission range of (400−730) nm. The samples were measured at 561 nm with beam splitters MBS at HFT 488/561, DBS1 at mirror and DBS2 NFT 565. The objective used for all the samples was EC Plan-Neofluar 40X/0.75, except for f-SHS@DTR-3, f-SHS@mCh, and beads@DTR-3 in which the objective used was Plan-Apochromat 63X/1.40 oil DIC M27. The emission filter of BP (Band Pass) 575−615 nm IR was used for f-SHS, f-SHS@DTR-3, f-SHS@DTR-10, f-SHS@DTR-70, beads, and beads@DTR-3. In the case of f-SHS@Dox, f-SHS@Cyt, f-SHS@RhB, and f-SHS@mCh, the emission filter was LP (long pass) 575 nm.

Dynamic Light Scattering (DLS). The hydrodynamic size of the particles at 25.0 ± 0.1 °C was obtained using a Zetasizer Nano ZS (model ZEN3600) from Malvern Instruments Ltd. with a 4 mW laser of 632.8 nm wavelength and a backscatter angle of 173°. The dispersant used was PBS 1X at pH 7.4 with a dispersant refractive index (RI) of 1.332 and viscosity of 0.9074 cP at 30.0 °C. For all the samples of f-SHS, f-SHS with encapsulated cargo, doxorubicin control, and rhodamine b control alone, the material RI was chosen as 1.00 as the default. In the case of the controls of pGFP, pCrimson, mCherry, DsRed, Cytochrome c, and Ovalbumin, the material RI used was 1.45 for the protein model. In the case of each control of dextrans (3 kDa, 10 kDa, and 70 kDa) conjugated with Texas red, the material RI model used was 1.47 from the cellulose model. For the bead controls (alone and with encapsulated DTR-3), the material RI was 1.590 using the polystyrene latex model. The D_H values are an average from 11 runs with equilibration time of 60 s and an analysis model of multiple narrow modes at high resolution provided by the instrument software (Malvern Zetasizer Software version 7.10).

Zeta Potential. These measurements were performed in the Zetasizer Nano ZS (model ZEN3600) from Malvern Instruments Ltd.
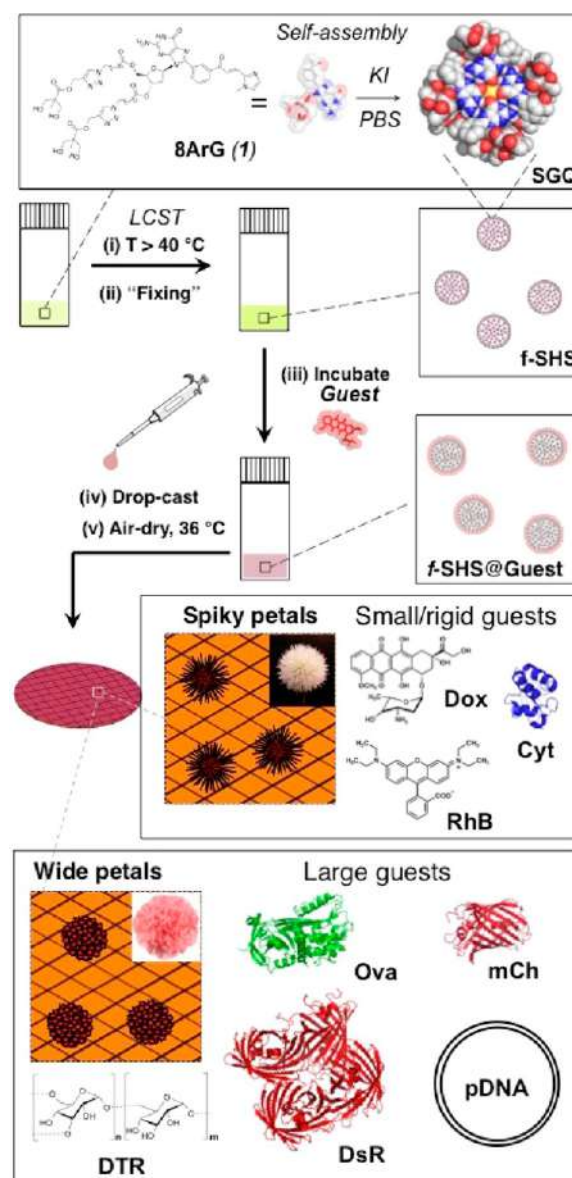

Figure 1. Preparative protocol for f-SHS and the corresponding nanoflowers (NFs). 8ArG self-assembly into SGQs followed by the (i) formation of SHS by LCST, is followed by (ii) decreasing the ionic strength to "fix" (i.e., kinetically stabilized) the SHS (identified as f-SHS). (iii) The encapsulation method relies on an osmotic gradient to form f-SHS@Guest complexes, and is suitable for the complexation of sensitive guests like proteins, which could be denatured by the initial high ionic strengths. (iv−v) Drop casting the solutions of f-SHS@Guest followed by air-drying leads to the formation of two families of NFs, having either spiky or wide petals as a result of complexing small or large guests, respectively. Some groups in the space filling representation of **1** (e.g., imidazole moiety) are omitted for clarity. We represent complexed guests with an "@", for example, f-SHS with encapsulated DTR 3 kDa is represented as f-SHS@DTR-3 where "3" is the molecular weight of the DTR in kDa.

at zeta potential mode with the same material and dispersant RI values used for the DLS experiments at 25.0 ± 0.1 °C. The measurements were processed by the instrument software with an analysis auto mode model and the Smoluchowski equation with an F (κa) value of 1.50 at 25.0 °C.[18]

■ RESULTS AND DISCUSSION

Although the formation of the SHS particles is reversible (e.g., by cooling the solution below the LCST), lowering the ionic
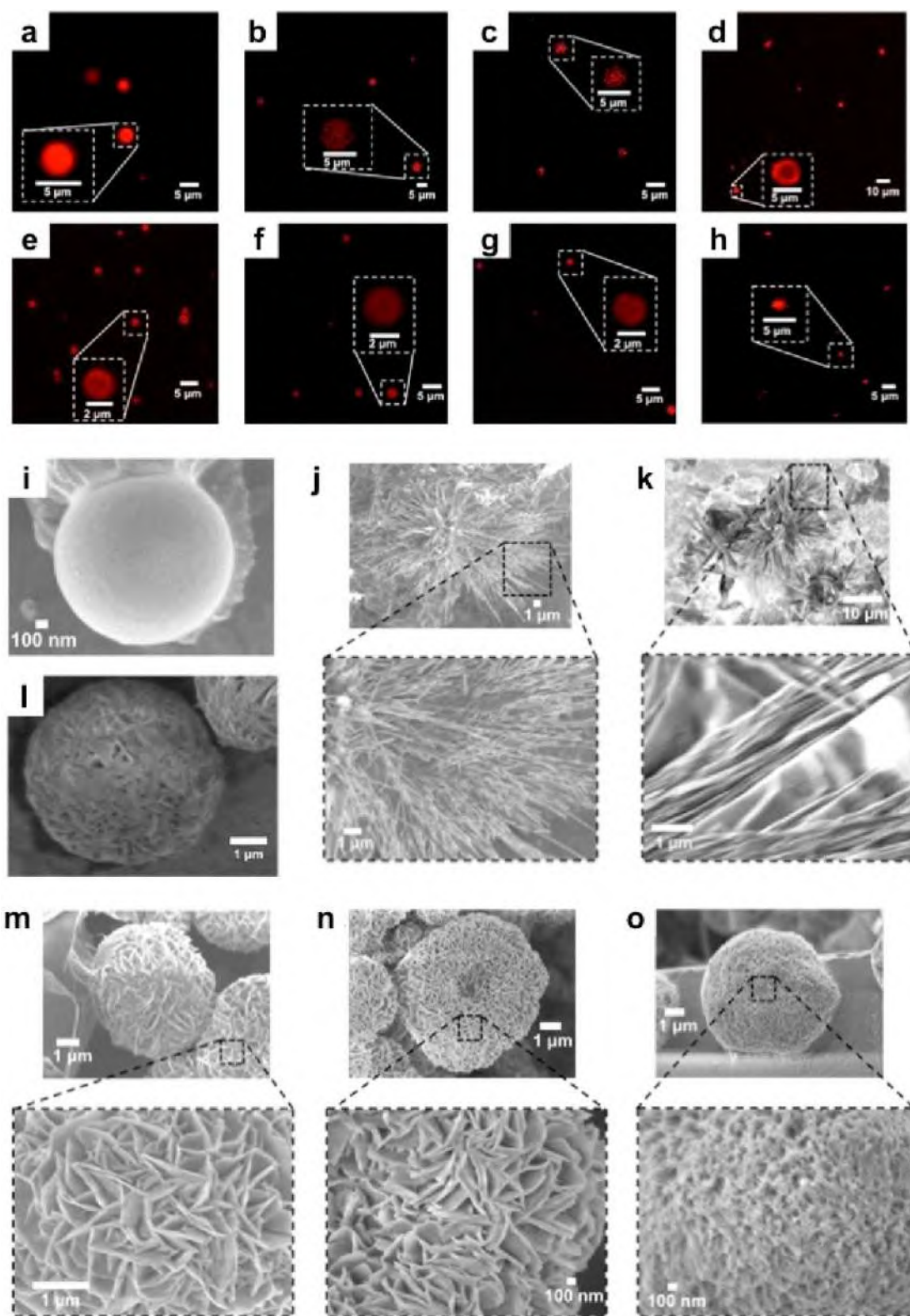
Figure 2. Microscopy images of *f*-SHS@Guest: (a−h) in solution by CLSM, and in (i−o) the solid state by SEM. The guests corresponding to each image are (a) RhB; (b) Dox; (c) Cyt; (d) DsR; (e) DTR-3; (f) DTR-10; (g) DTR-70; (h) mCh. SEM images correspond to (i) *f*-SHS alone; (j) *f*-SHS@ Dox; (k) *f*-SHS@RhB; (l) lyophilized *f*-SHS; (m) *f*-SHS@DTR-3; (n) *f*-SHS@DTR-10; (o) *f*-SHS@DTR-70. The SEM images were drop-casted from a solution of 8ArG (0.303 mM, 121 mM KI, in 1X PBS, pH 7.4) and air-dried at 36 °C.

strength of the colloidal suspension leads to the formation of kinetically stable or "fixed" SHS (*f*-SHS) that tolerates a wide range of physical manipulations (e.g., dilution, deposition). The porous gel-like architecture of the *f*-SHS is revealed by SEM measurements of freeze-dried samples (Figure 2i−o), which explains the facile diffusion and encapsulation of guest molecules like the fluorescent anticancer drug doxorubicin (Dox) as previously reported by our group.[17b]
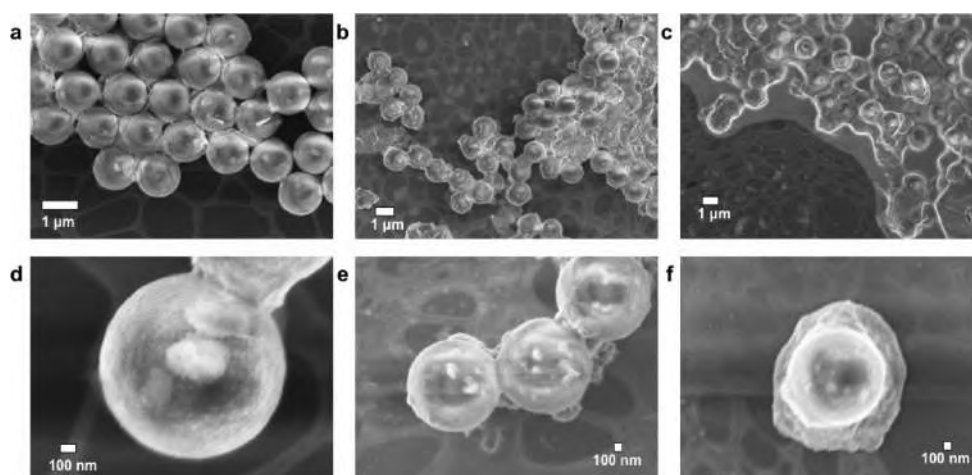
Figure 3. SEM images of 0.303 mM polystyrene beads (PSBs) used for control experiments. (a) PSBs alone (X14000); (b) PSBs + DTR-3 (5 equiv; 0.07 mM; X7000); (c) PSBs + RhB (10 equiv; 3.4 mM; X6000). (d−f) Zooms of a, b, and c at (d) X60000; (e) X30000; and (f) X30000, respectively. All the samples were air-dried at 36 °C after incubating for 1 h with the indicated guest molecule.

In order to understand the diffusion through the *f*-SHS, we studied the encapsulation of dextran labeled with Texas Red (DTR) in three different sizes (molecular weights: 3 kDa, 10 kDa, 70 kDa).[19] CLSM revealed these *f*-SHS complexes to be similar to those described earlier using Dox (in situ method; Figure 2a).[17b] We then evaluated how DTR encapsulation affected the morphology of the *f*-SHS in the solid state by drop-casting the samples over a copper grid (air-dried at 36 °C) and visualizing them by SEM, which resulted in the discovery of flower-like structures like those in Figure 2.

Control experiments revealed that NFs are not formed in the absence of *f*-SHS (e.g., DTRs alone; see Figures S26−29) or by empty *f*-SHS (Figure 2i) in samples treated under otherwise identical conditions to those reported earlier for *f*-SHS@DTRs. Furthermore, the presence of polystyrene beads (PSBs), which have size, porosity, and zeta potential (ZP) similar to that of the *f*-SHS, was not effective in promoting the formation of NFs. Considering the PSBs can encapsulate DTR-3 (PSBs@DTR-3; Figure 3), we hypothesize that the fact that they are not suitable templates for NF formation is, at least in part, due to their different internal organization relative to the *f*-SHS, which suggests that the supramolecular structure of the latter is a key feature of the system.

Intrigued by the aforementioned observations, we set out to determine the scope and limitations of this phenomenon via the encapsulation in the *f*-SHS, and subsequent surface deposition methodology, of a broad variety of molecules with a wide range of sizes, shapes, and other physicochemical properties. First, we examined the construction of NFs from fluorescent small molecules suitable for biologically relevant applications in drug-delivery such as Dox and imaging probes elaboration like rhodamine B (RhB).[17b,20] Both molecules lead to the formation of spiky-petalled (sp) NFs, instead of the wide-petalled (wp) NFs formed by *f*-SHS@DTRs (Figure 2), despite their different ZP values (RhB −25.3 mV; DOX + 9.5 mV; Supplementary Table S4). Nevertheless, both NFs show some differences, most saliently, the spiky shaped petals of the *f*-SHS@Dox NFs have a helical morphology, while the *f*-SHS@RhB NFs are better described as bundles of straight fibers (Figure 2).

The two families of guest compounds tested up to this point left molecular size and flexibility as the potential key parameters driving the final morphological transformation of the *f*-SHS particles,

with small/rigid (e.g., DOX) and large/flexible (e.g., DTR) promoting sp-NFs versus wp-NFs, respectively. In order to clarify this, we tested the complexes of proteins of increasing sizes, which span a relatively large size range but with little flexibility relative to DTR polymers. At the lowest and highest values of sizes we evaluated cytochrome c (Cyt) and DsRed2 (DsR), with mCherry (mCh) and Ovalbumin (Ova) in the intermediate range. We also chose these set of proteins because of their use in biomedical applications[19] like molecular probes (e.g., mCh, DsR)[21−23] vaccine development studies (e.g., Ova),[24] and experimental anticancer treatments (Cyt).[25,26]

The *f*-SHS@Cyt formed NFs with fibrillar (nonhelical) spiky petals resembling those formed by *f*-SHS@RhB NFs. Larger proteins such as mCh and DsR lead to the formation of wp-NFs, resembling those induced by the DTR guests, but with a different petalled surface pattern (Figure 4b). Ova, on the other hand, lead to the formation of different type of "brain-like" structures (Figure 4c), but increasing the drying temperatures to 65 °C resulted in irregularly shaped "carnation-like" NFs (Figure 4h) with surface patterns similar to those induced by DTR-3 and DTR-10. We hypothesize that the increase hydrophobicity of Ova could be responsible for its preferential deposition on the glassy carbon regions of the grid after drying at 36 °C.

The sizes of the *f*-SHS particles and the various complexes studied (*f*-SHS@guest) remain fairly constant for the first 2 h after their preparation (Figure S34). While there does not appear to be broad trends between the sizes (or molecular weights) of the various *f*-SHS@guest particles, there seem to be a number of tendencies within family of guests. The clearest tendency is that within DTR series, where the size of the resulting *f*-SHS@guest particles is inversely proportional to that of the guest (DTR-3: 1246 nm; DTR-10: 949 nm; DTR-70: 679 nm; Tables S3 and S4). There is in fact a propensity for smaller guests to promote larger particles, perhaps as a consequence of greater swelling due to increased penetration of the smaller guests. Nevertheless, while the smallest protein (Cyt) does result in the largest particle of the protein series (3892 nm; Tables S3 and S4), the second largest corresponds to *f*-SHS@DsR (2275 nm; Tables S3 and S4), which is the largest protein studied. These results indicate that other parameters, beyond guest size (e.g., hydrophobic character, geometry) likely play an important role in determining the sizes of the resulting particles. The zeta potential (ZP), however, does not
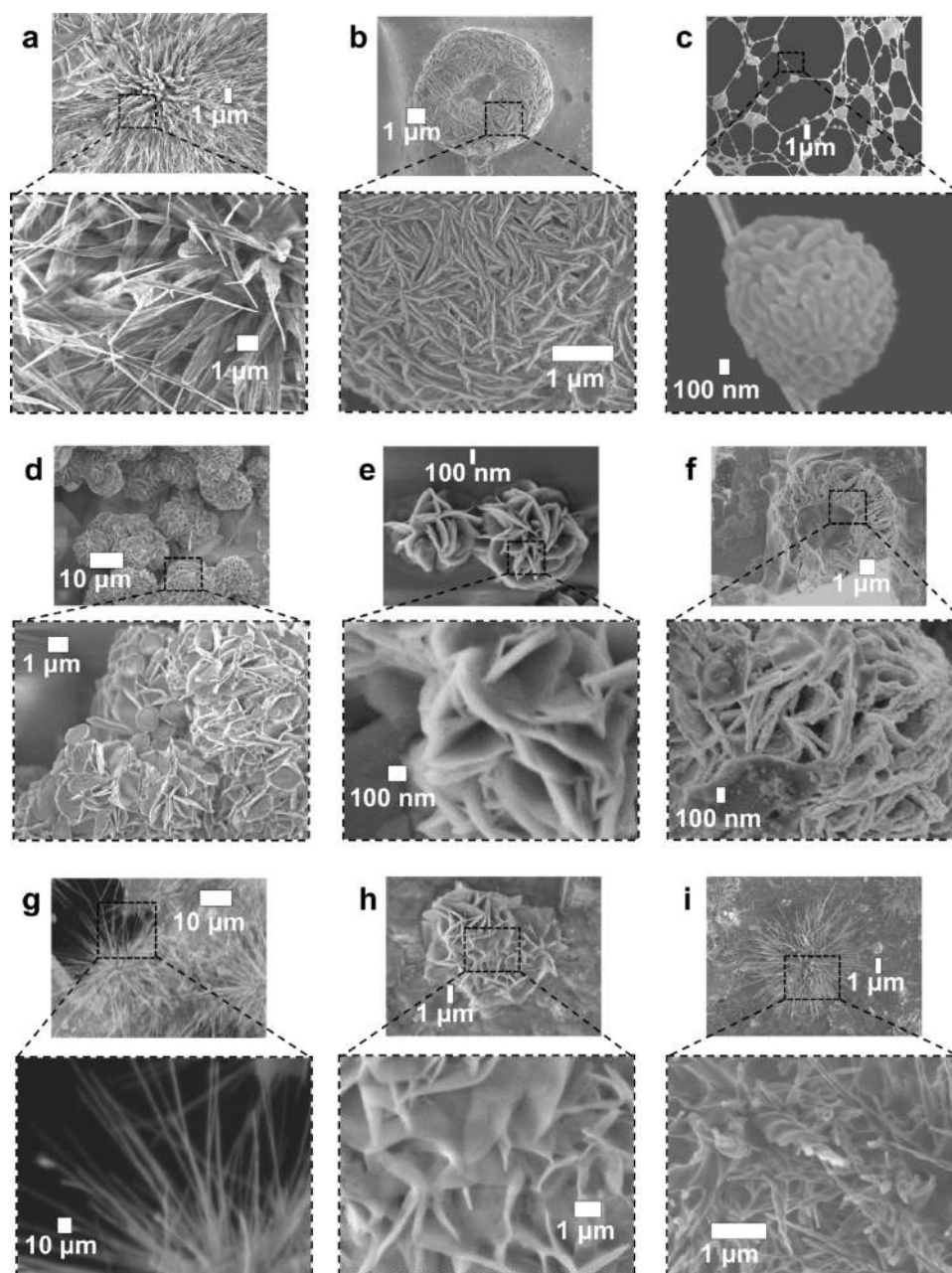
Figure 4. SEM images of different organic NFs after air-drying at 36 °C (a−f) and 65 °C (g−i). Protein guests: (a) *f*-SHS@Cyt; (b) *f*-SHS@mCh; (c) *f*-SHS@Ova; (d) *f*-SHS@DsR. pDNA guests: (e) *f*-SHS@pCri, (f) *f*-SHS@pGFP; (g) *f*-SHS alone. Protein guest: (h) *f*-SHS@Ova; small molecule guest: (i) *f*-SHS@RhB. The NFs from *f*-SHS@Ova (c) were observed primarily on the carbon section of the SEM grid, in contrast to the rest of NFs studied, which formed on the copper section of the grid.

seem to be a critical parameter determining the size of the particles, given that the *f*-SHS seems to neutralize the ZPs of the resulting complexes considering their values to a relatively narrow range (Tables S3 and S4).

A higher air-drying temperature (i.e., 65 °C instead of 36 °C) could be used to modify the surface morphology of the resulting NF as described for *f*-SHS@Ova. Under the same conditions the NFs promoted by DTRs, mCh, DsR, and pDNAs preserve the wide-petal-shaped surface patterns, albeit with expanded groove sizes and with distorted globular shapes relative to their counterparts at 36 °C (Figures S8−S24). Both *f*-SHS@Dox and *f*-SHS@Cyt were transformed into NFs with straight spikes, in contrast to the helical spikes observed at 36 °C (Figures 2j, S4). By contrast, the *f*-SHS@RhB went from straight to helical sp-NFs

(Figure 3i). Interestingly, air-drying of the *f*-SHS at 65 °C with no added guests, led to their transformation from spherical particles (Figure 2i) to dandelion-like NFs (Figure 4g). We hypothesize that, at this higher temperature (just below the disassembly temperature for these SGQs in solution),[17a] this transformation results from the transition of the *f*-SHS constituent SGQ structures from stacks of planar tetramers to ribbon-like assemblies as has been described for related lipophilic guanosine derivatives.[27]

Finally, we tested the complexation of plasmid DNA (pDNA) because, relative to all other tested macromolecules, it has a unique topology, larger size, polyanionic character, and importance for biological applications. We used *f*-SHS to complex plasmids encoding for fluorescent proteins like E2-Crimson (pCrimson; pCri) and green fluorescent protein (pGFP). Both of the resulting
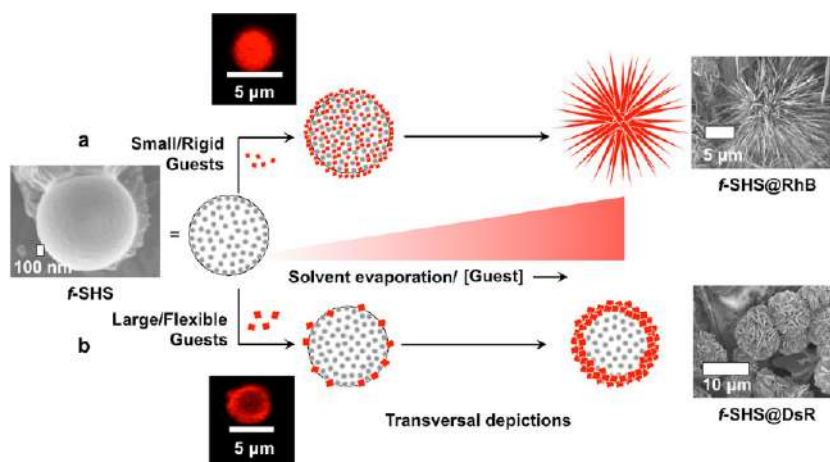
Figure 5. Mechanistic hypothesis for the formation of organic NFs from the *f*-SHS@Guest complexes: (a) For small/rigid guests like RhB, the guest diffuses throughout the porous *f*-SHS by osmotic gradient until it fills the gel-like interior. Upon removing the solvent (e.g., 36 or 65 °C), the concentration of guest increases, which lead to enhanced noncovalent interactions resulting in the spiky NFs from *f*-SHS@RhB. This seems to promote a crystallization growth perpendicular to the particle's surface leading to the formation of spiky-petalled NFs. (b) Larger or more flexible guests like DsR are concentrated on or near the surface of the *f*-SHS favoring the formation of the wide-petalled NF surface in *f*-SHS@DsR.
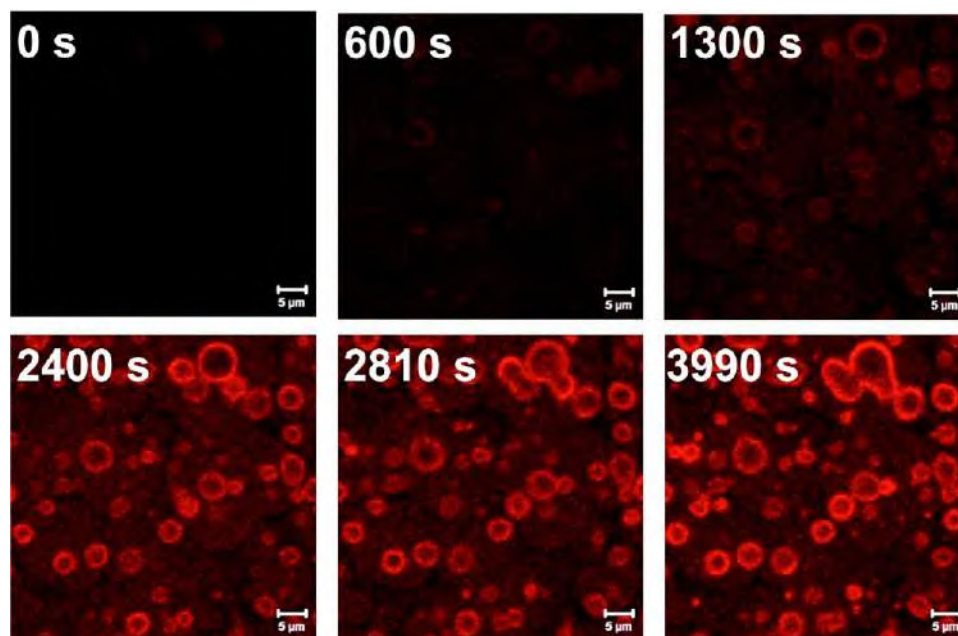
Figure 6. Time course CLSM images of *f*-SHS incubated with DTR-3 (5 equiv., 0.07 mM). Images at 0 s, 600 s (10 min), 1300 s (21.7 min), 2400 s (40 min), 2810 s (46.8 min), and 3990 s (1.1 h). The images were taken with an EC Plan-Neofluar 40X/0.75 objective, excitation wavelength of 561 nm and an emission filter of LP 575 (25 °C). The *f*-SHS were prepared from following the conditions described in Figures 2 and 3.

complexes, *f*-SHS@pCri and *f*-SHS@pGFP, formed rose-like NFs after air-drying at 36 °C (Figure 4e,f).[28] While polycationic DNA nonviral delivery systems[23,24] are known to induce the formation of toroids, rods, and tangled fibers (some of which are reminiscent of a 2D-flower),[29] the rose-like morphology presented here is unprecedented for a pDNA complex.

While the specific surface patterns of these NFs show some variety, all the aforementioned NFs fall in two broad categories: spiky-petalled (acute-shaped elongated petals like those of dandelions, dahlias, and globe thistles) and wide-petalled (e.g., petals with oblong, or ovate/obovate shapes like carnations, peonies, and roses).[6] We propose that the geometry of wp-NFs results from guest clustering into 2-D crystalline domains, while the sp-NFs result from the corresponding guest clustering into spiky 1-D crystalline domains. The experimental evidence shows

that the former are favored by larger and/or flexible guests while the latter are promoted by smaller and/or rigid guests (Figure 5).

Considering the wide variety of guest molecules (e.g., chemical composition, size, shapes) it is remarkable to obtain just two types of morphologies. But, what drives the formation of these NFs, in general, and how can we explain the two broad types of morphologies in particular? Our previous work[17a] suggest that the gel-like interior of the *f*-SHS is composed of well-defined supramolecules (i.e., SGQs), which we hypothesize provide nucleation sites where noncovalent interactions promote the formation of the final morphology (Figure 5). In our proposed model, rigid guests small enough to freely diffuse deep into the *f*-SHS concentrate in the channels of the gel like interior (Figure 5a). Solvent evaporation in the channels promotes the formation of nanocrystalline domains of the encapsulated guest,

which continue to grow beyond, and perpendicular to, the surface of the *f*-SHS. This putative process is reminiscent of the reported nucleation and perpendicular growth of supramolecular oligothiophene bundled fibers through a porous aluminum oxide membrane[30] and the hierarchical self-assembly of dipeptides into dandelion-like microstructures.[31] Furthermore, due to the supramolecular nature of *f*-SHS template, we hypothesize that guest crystallization in the channels induces a clustering and rearrangement[32] of the entire complex (*f*-SHS@guest) in order to optimize noncovalent interactions (e.g., minimize repulsive and maximize attractive). Specific features such as the helicity of the spiky petals are likely due to the chirality of the molecular components of the *f*-SHS (i.e., 8ArG subunits) and most guests (all except RhB).

An alternative mechanism for the formation of the NFs could involve a guest-induced disassembly and subsequent rearrangement leading to an intertwined hybrid composition. This process would be driven by the evaporation of the solvent, mediated by attractive noncovalent interactions between the constituents of the *f*-SHS and the complexed guests. Further studies, such as real-time in situ atomic force microscopy (AFM),[33] could provide useful insights to distinguish between this mechanism, the one described earlier (Figure 5), or some unforeseen alternatives.

Larger and/or flexible guests seem to aggregate primarily on or near the surface as illustrated by time course CLSM measurements with *f*-SHS incubated with DTR-3 (Figure 6), where the crystallization seems to occur parallel to the surface, but still influenced by the supramolecular components that make up the *f*-SHS (Figure 5b). Here too, the resulting hierarchical organization, from the nano- to the microscale, is driven by a synergistic interplay between equilibrium and nonequilibrium self-assembly where molecule–water (dewetting), molecule–substrate (adsorption) and molecule–molecule (deposition) interactions play critical roles.[34,35] These phenomena have parallels in reports describing template directed crystallization by diblock copolymers,[36] amyloid fibers,[37] and copper(II) ions.[36] The topography and curvature on the particle surface may also play a role in determining the interactions of the adsorbed guests as reported for other particle–protein systems (e.g., albumin, fibrinogen).[35,38]

CONCLUSIONS

Herein, we describe a general method to construct organic NFs from a wide variety of molecules using *f*-SHS particles as templates. The methodology's versatility is demonstrated by the mild conditions needed for the formation of NFs from a wide variety of biologically relevant molecules, with a large range of sizes, charges and other physicochemical characteristics. The gel-like interior enabled by the hierarchical supramolecular structure of the *f*-SHS seems to strike a balance between being flexible and rigid enough to adapt to such disparate guests, while supporting well-defined morphological features. We are currently evaluating how other parameters such as 8ArG structure, hydrophobicity, stronger charge–charge interactions and different guest combinations affect the specific morphological features of these NFs. We expect these results to jump-start the development of organic NFs for applications in areas like biocatalysis,[1] drug delivery[2] and other biologically relevant applications. Recent results from our group indicate that the *f*-SHS@Dox as well as *f*-SHS@pGFP and *f*-SHS@pCri are suitable for the delivery of anticancer drugs and genes into cells, respectively. A full account of these results will be published in due course.

ASSOCIATED CONTENT

Supporting Information

The Supporting Information is available free of charge on the ACS Publications website at DOI: 10.1021/acs.langmuir.5b03946.

> Corresponding controls of the performed SEM and CLSM experiments. Other experiments performed were DLS and zeta potential with the corresponding controls. (PDF)

AUTHOR INFORMATION

Corresponding Author

*E-mail: riveralab.upr@gmail.com.

Notes

The authors declare no competing financial interest.

REFERENCES

(1) Ge, J.; Lei, J.; Zare, R. N. Protein-inorganic hybrid nanoflowers. *Nat. Nanotechnol.* **2012**, 7 (7), 428–432.

(2) Hu, X.; Hu, J.; Tian, J.; Ge, Z.; Zhang, G.; Luo, K.; Liu, S. Polyprodrug amphiphiles: hierarchical assemblies for shape-regulated cellular internalization, trafficking, and drug delivery. *J. Am. Chem. Soc.* **2013**, 135 (46), 17617–17629.

(3) Lee, J. B.; Hong, J.; Bonner, D. K.; Poon, Z.; Hammond, P. T. Self-assembled RNA interference microsponges for efficient siRNA delivery. *Nat. Mater.* **2012**, 11 (4), 316–322.

(4) Lee, J. B.; Peng, S.; Yang, D.; Roh, Y. H.; Funabashi, H.; Park, N.; Rice, E. J.; Chen, L.; Long, R.; Wu, M.; Luo, D. A mechanical metamaterial made from a DNA hydrogel. *Nat. Nanotechnol.* **2012**, 7 (12), 816–820.

(5) Kharisov, B. I. A review for synthesis of nanoflowers. *Recent Pat. Nanotechnol.* **2008**, 2 (3), 190–200.

(6) Coen, E.; Rolland-Lagan, A.-G.; Matthews, M.; Bangham, J. A.; Prusinkiewicz, P. The genetics of geometry. *Proc. Natl. Acad. Sci. U. S. A.* **2004**, 101 (14), 4728–4735.

(7) Huang, Y.; Ran, X.; Lin, Y.; Ren, J.; Qu, X. Self-assembly of an organic-inorganic hybrid nanoflower as an efficient biomimetic catalyst for self-activated tandem reactions. *Chem. Commun.* **2015**, 51 (21), 4386–4389.

(8) Lin, Z.; Xiao, Y.; Wang, L.; Yin, Y.; Zheng, J.; Yang, H.; Chen, G. Facile synthesis of enzyme–inorganic hybrid nanoflowers and their application as an immobilized trypsin reactor for highly efficient protein digestion. *RSC Adv.* **2014**, 4, 13888–13891.

(9) Zhu, G.; Hu, R.; Zhao, Z.; Chen, Z.; Zhang, X.; Tan, W. Noncanonical self-assembly of multifunctional DNA nanoflowers for biomedical applications. *J. Am. Chem. Soc.* **2013**, 135 (44), 16438–16445.

(10) Wang, L.-B.; Wang, Y.-C.; He, R.; Zhuang, A.; Wang, X.; Zeng, J.; Hou, J. G. A new nanobiocatalytic system based on allosteric effect with dramatically enhanced enzymatic performance. *J. Am. Chem. Soc.* **2013**, 135 (4), 1272–1275.

(11) Xiao, Y.; Zhang, M.; Wang, F. X.; Pan, G. B. Hierarchical flower-shaped organic NPB architectures with a durable water-repellent property. *CrystEngComm* **2012**, 14, 1933–1935.

(12) Karan, S.; Mallik, B. Nanoflowers grown from phthalocyanine seeds: Organic nanorectifiers. *J. Phys. Chem. C* **2008**, 112 (7), 2436–2447.

(13) Nakanishi, T.; Ariga, K.; Michinobu, T.; Yoshida, K.; Takahashi, H.; Teranishi, T.; Möhwald, H.; Kurth, D. G. Flower-shaped

supramolecular assemblies: hierarchical organization of a fullerene bearing long aliphatic chains. *Small* **2007**, *3* (12), 2019−2023.

(14) Zhao, H.; Guo, X.; He, S.; Zeng, X.; Zhou, X.; Zhang, C.; Hu, J.; Wu, X.; Xing, Z.; Chu, L.; He, Y.; Chen, Q. Complex self-assembly of pyrimido[4,5-d]pyrimidine nucleoside supramolecular structures. *Nat. Commun.* **2014**, *5*, 3108.

(15) Yin, J.; Yan, J.; He, M.; Song, Y.; Xu, X.; Wu, K.; Pei, J. Solution-processable flower-shaped hierarchical structures: self-assembly, formation, and state transition of biomimetic superhydrophobic surfaces. *Chem. - Eur. J.* **2010**, *16* (24), 7309−7318.

(16) Davis, J. T.; Spada, G. P. Supramolecular architectures generated by self-assembly of guanosine derivatives. *Chem. Soc. Rev.* **2007**, *36* (2), 296−313.

(17) (a) Betancourt, J. E.; Rivera, J. M. Nonpolymeric Thermosensitive Supramolecules. *J. Am. Chem. Soc.* **2009**, *131* (46), 16666−16668. (b) Betancourt, J. E.; Subramani, C.; Serrano-Velez, J. L.; Rosa-Molinar, E.; Rotello, V. M.; Rivera, J. M. Drug encapsulation within self-assembled microglobules formed by thermoresponsive supramolecules. *Chem. Commun.* **2010**, *46* (45), 8537−8539.

(18) Sze, A.; Erickson, D.; Ren, L.; Li, D. Zeta-potential measurement using the Smoluchowski equation and the slope of the current−time relationship in electroosmotic flow. *J. Colloid Interface Sci.* **2003**, *261* (2), 402−410.

(19) Vermonden, T.; Censi, R.; Hennink, W. E. Hydrogels for Protein Delivery. *Chem. Rev.* **2012**, *112* (5), 2853−2888.

(20) Farag, A. A. M.; Yahia, I. S. Structural, absorption and optical dispersion characteristics of rhodamine B thin films prepared by drop casting technique. *Opt. Commun.* **2010**, *283* (21), 4310−4317.

(21) Baird, G. S.; Zacharias, D. A.; Tsien, R. Y. Biochemistry, mutagenesis, and oligomerization of DsRed, a red fluorescent protein from coral. *Proc. Natl. Acad. Sci. U. S. A.* **2000**, *97* (22), 11984−11989.

(22) Shaner, N. C.; Steinbach, P. A.; Tsien, R. Y. A guide to choosing fluorescent proteins. *Nat. Methods* **2005**, *2* (12), 905−909.

(23) Wall, M. A.; Socolich, M.; Ranganathan, R. The structural basis for red fluorescence in the tetrameric GFP homolog DsRed. *Nat. Struct. Biol.* **2000**, *7* (12), 1133−1138.

(24) Smith, D. M.; Simon, J. K.; Baker, J. R. Applications of nanotechnology for immunology. *Nat. Rev. Immunol.* **2013**, *13* (8), 592−605.

(25) Méndez, J.; Morales Cruz, M.; Delgado, Y.; Figueroa, C. M.; Orellano, E. A.; Morales, M.; Monteagudo, A.; Griebenow, K. Delivery of Chemically Glycosylated Cytochrome c Immobilized in Mesoporous Silica Nanoparticles Induces Apoptosis in HeLa Cancer Cells. *Mol. Pharmaceutics* **2014**, *11* (1), 102−111.

(26) Slowing, I. I.; Trewyn, B. G.; Lin, V. S. Y. Mesoporous Silica Nanoparticles for Intracellular Delivery of Membrane-Impermeable Proteins. *J. Am. Chem. Soc.* **2007**, *129* (28), 8845−8849.

(27) Spada, G. P.; Lena, S.; Masiero, S.; Pieraccini, S.; Surin, M.; Samorì, P. Guanosine-based Hydrogen-bonded Scaffolds: Controlling the Assembly of Oligothiophenes. *Adv. Mater.* **2008**, *20* (12), 2433−2438.

(28) Golan, R.; Pietrasanta, L. I.; Hsieh, W.; Hansma, H. G. DNA Toroids: Stages in Condensation. *Biochemistry* **1999**, *38* (42), 14069−14076.

(29) Fang, Y.; Hoh, J. H. Early intermediates in spermidine-induced DNA condensation on the surface of mica. *J. Am. Chem. Soc.* **1998**, *120* (35), 8903−8909.

(30) Tevis, I. D.; Palmer, L. C.; Herman, D. J.; Murray, I. P.; Stone, D. A.; Stupp, S. I. Self-Assembly and Orientation of Hydrogen-Bonded Oligothiophene Polymorphs at Liquid−Membrane−Liquid Interfaces. *J. Am. Chem. Soc.* **2011**, *133* (41), 16486−16494.

(31) Wang, Y.; Huang, R.; Qi, W.; Xie, Y.; Wang, M.; Su, R.; He, Z. Capillary Force-Driven, Hierarchical Co-Assembly of Dandelion-Like Peptide Microstructures. *Small* **2015**, *11*, 2893−2902.

(32) Madras, G.; McCoy, B. J. A distribution kinetics model of self-assembly: Effects of coalescence and solvent evaporation. *J. Cryst. Growth* **2006**, *286* (1), 131−136.

(33) Shtukenberg, A. G.; Zhu, Z.; An, Z.; Bhandari, M.; Song, P.; Kahr, B.; Ward, M. D. Illusory spirals and loops in crystal growth. *Proc. Natl. Acad. Sci. U. S. A.* **2013**, *110* (43), 17195−17198.

(34) Palermo, V.; Samori, P. Molecular Self-Assembly across Multiple Length Scales. *Angew. Chem., Int. Ed.* **2007**, *46* (24), 4428−4432.

(35) Mann, S. Self-assembly and transformation of hybrid nano-objects and nanostructures under equilibrium and non-equilibrium conditions. *Nat. Mater.* **2009**, *8* (10), 781−792.

(36) Hahm, J.-i. Fundamentals of Nanoscale Polymer−Protein Interactions and Potential Contributions to Solid-State Nanobioarrays. *Langmuir* **2014**, *30* (33), 9891−9904.

(37) Linse, S.; Cabaleiro-Lago, C.; Xue, W.-F.; Lynch, I.; Lindman, S.; Thulin, E.; Radford, S. E.; Dawson, K. A. Nucleation of protein fibrillation by nanoparticles. *Proc. Natl. Acad. Sci. U. S. A.* **2007**, *104* (21), 8691−8696.

(38) Kurylowicz, M.; Paulin, H.; Mogyoros, J.; Giuliani, M.; Dutcher, J. R. The effect of nanoscale surface curvature on the oligomerization of surface-bound proteins. *J. R. Soc., Interface* **2014**, *11* (94), 20130818.